Journal of Wood Science

NOTE

Open Access

Liquid-phase water permeation pathways on outer-bark surfaces of teak (*Tectona grandis*): a tropical deciduous hardwood

Hiroyuki Matsunaga[1*], Naoko Matsuo[1], Takahisa Nakai[1] and Hisashi Abe[2]

Abstract

It has recently been suggested that processes related to water uptake from the tree-stem surface, such as water vapor exchange and rainwater permeation, have implications for forest hydrology. However, few studies have investigated stem surface water uptake itself, and the water permeation pathway has not been elucidated in detail. Based on previous findings that trees with outer bark composed mainly of rhytidome have a high frequency of exfoliation and greater water uptake ability, we hypothesized that exfoliation of the outer bark is the main pathway for water uptake from the outer bark surface to the innermost periderm in these species. We tested this hypothesis in teak, a tropical deciduous hardwood with a high frequency of outer-bark exfoliation. We conducted laboratory experiments using dried bark pieces with different outer-bark shapes to evaluate the rate, amount, and pathway of liquid-phase water permeation of outer-bark surfaces. The rate and amount of water absorption differed markedly among samples. The permeation rate was correlated with the degree of outer-bark exfoliation, and water permeation was observed to begin at exfoliated surfaces. These results support our hypothesis. In addition, the increased water content of bark pieces immediately after the start of the experiment was strongly correlated with the surface roughness of the outer bark, implying that roughness may indicate the water-retention capacity of a given tree species.

Keywords Bark, Forest hydrology, Outer-bark shape, Rainwater interception, Water uptake

Introduction

In woody plants, bark is a tissue outside the vascular cambium that is composed of inner bark (phloem) derived from the vascular cambium, and outer bark that lies outside the innermost periderm and is composed of phelloderm and phellem derived from phellogen [1–3]. The inner bark is responsible for the transport and storage of photosynthetic assimilates and signaling molecules, whereas the outer bark, which is partially made of rhytidome (alternating layers of phellem and collapsed phloem), protects the inner tissue from fire, physical damage, disease, and herbivores [1–3]. The morphology of bark, particularly outer bark, varies significantly among species, and these differences affect its various protective roles [4–6].

Phellem in outer bark contains hydrophobic components such as suberin and waxes, which maintain lower equilibrium moisture content and water vapor diffusivity compared to xylem and inner bark, where water vapor is adsorbed and desorbed [7–10]. The low permeability of liquid-phase water and water vapor is assumed to play a role in preventing water loss in terrestrial plants [11–14]. However, several studies have supported the notion of water uptake via the stem surface. In this paper, we define water uptake via the stem (or outer-bark) surface as the net uptake from liquid-phase water and water

*Correspondence:
Hiroyuki Matsunaga
521d101@m.mie-u.ac.jp
[1] Graduate School of Bioresources, Mie University, 1577 Kurimamachiya, Tsu, Mie 514-8507, Japan
[2] Forestry and Forest Products Research Institute, 1 Matsunosato, Tsukuba, Ibaraki 305-8687, Japan

vapor exchange on this surface. This was first observed during a laboratory experiment in which distilled water or dye solution was sprayed onto the surfaces of *Picea abies* branches [15]. In another laboratory experiment, freshly cut and defoliated *Sequoia sempervirens* and *Salix matsudana* branches were submerged, and functional recovery of xylem water transport occurred through such uptake [16, 17]. Furthermore, it has been suggested that living *Taxodium distichum* trees absorb fog through branch surfaces [18], and field experiments using intact tree branches wrapped in water-soaked cotton wool have suggested that *Pinus sylvestris* and *Fagus sylvatica* trees also absorb water in this manner [19]. These findings also imply that water uptake via the stem surface affects trees' water use. However, despite increasing recognition of this process in recent years, its detailed mechanism is largely unclear and whether it occurs generally or under specific environmental conditions and/or in specific tree species remains unknown [19–21]. Therefore, detailed elucidation of this process is needed to understand its significance in forest hydrology [20, 21].

The pathway of water uptake via the stem surface has not been clarified [16, 20]. Radial tissue running between the xylem and the inner bark is interrupted by phellem, creating physiological discontinuity between the outer bark and the stem interior [3]. In the outer bark of *Betula pendula*, which is thin and composed mainly of periderm, the hydrophilic portion of the phellem cell wall has been reported to be a water-uptake pathway [22]. On the other hand, the outer bark surface and the innermost periderm in trees with well-developed rhytidome are separated by a thick layer of dead tissue, and the pathway of water permeation between them remains unknown. In a recent laboratory experiment, bark pieces sealed on all sides except the outer-bark surface were submerged in water, and markedly higher water absorption rates and amounts were observed in species with fibrous outer bark, particularly those with rough surfaces [23]. Among live trees growing in the same area, water-uptake rates at the branch surface were higher in *P. sylvestris* than in *F. sylvatica* [19]. The outer bark of *Pinus pinea*, which has similar morphology to that of *P. sylvestris*, is composed of rhytidome, which is characterized by high exfoliation frequency and a rough surface [24]; that of *F. sylvatica* is composed mainly of periderm, which has a lower exfoliation frequency and a smoother surface [25]. The ratio of outer-bark thickness to stem diameter was recently found to be negatively correlated with stem water vapor permeability in 10 savanna shrub species [26]. Considering these previous findings, we hypothesized that the capacities and pathways for water uptake from the outer-bark surface to the innermost periderm differ among species with different outer-bark morphologies. Many species that take up water through stem surfaces have outer bark consisting mainly of rhytidome that exhibits frequent exfoliation (e.g., *P. abies* in [15, 27]; *Picea glauca* in [28]; *P. sylvestris* in [19]; *S. sempervirens* in [16]; *T. distichum* in [18]). In addition, the rate of carbon dioxide exchange increases when the outer bark is exfoliated and fissured [29]. Physical damage to the periderm, which prevents the permeation of carbon dioxide along with liquid-phase water and water vapor, is thought to be responsible for this phenomenon [11, 12, 22]. Thus, such damage is thought to significantly reduce the capacity of outer bark to prevent liquid-phase water permeation. Therefore, we hypothesized that exfoliation of the outer bark is the main pathway for liquid-phase water permeation from the outer-bark surface to the innermost periderm in species with outer bark composed mainly of rhytidome.

In a previous study [30], we reported evidence supporting water exchange at the stem surface based on bark samples collected from a teak tree (*Tectona grandis* L. f.) in Mae Moh District, Lampang Province, northern Thailand. At the study site, increases in the trunk circumference of this deciduous hardwood tree due to water storage were observed immediately after short rainfall events during the dry season, despite inactive sap flow. In laboratory experiments, we dried pieces of teak bark, sealed them on all sides except the outer-bark surface, and maintained them under constant humidity. We observed changes in the weights and volumes of the pieces over time, which confirmed water vapor exchange between the bark and the atmosphere through the outer surface. These results imply that water vapor exchange is one factor driving the increase in stem water storage observed at the study site. However, liquid-phase water permeation of the teak outer-bark surface has not been directly tested.

The outer bark of teak is composed of rhytidome, and its surfaces are densely fissured due to frequent exfoliation [31]. As an initial step toward testing our hypothesis under a range of climatic conditions and in various tree species, we attempted to confirm our previous gaseous-phase findings for liquid-phase water using bark pieces of different shapes sampled from the Mae Moh plantation. We conducted laboratory experiments to evaluate the rate, amount, and pathway of liquid-phase water permeation from the outer-bark surface to the innermost periderm. Water uptake via the stem surface was assumed to involve the water potential gradient between the surface and interior of the bark [16, 21]. The water state of the phellem also varies, which in turn affects its water permeability [22, 32]. Therefore, to remove the effects of individual differences in the initial water state of bark pieces on liquid-phase water permeation, in our laboratory experiments we used oven-dried bark pieces with a uniform water state

to clarify the relationship between outer-bark shape and water permeation.

Methods

Plant material

The bark of a teak tree growing in a plantation in Mae Moh District, northern Thailand (18° 25′ N, 99° 43′ E, 380 m a.s.l.), was used for laboratory experiments. Bark-bearing stem disks (39.8 cm in diameter) were collected from the study site in March 2016, air-dried outdoors at the site, and then transported to Japan for further air-drying indoors, a total of 2 years and 8 months of air-drying. Bark was peeled from the disks using a chisel and cut into 24 small pieces (10 mm × 10 mm) using an electric circular saw. The average weight and thickness of the air-dried bark pieces were 1.21 g and 9.69 mm, respectively.

Water permeation experiments

Prior to the experiments, 18 bark pieces were oven-dried at 105 °C for 24 h (DK:400 T; Yamato Science, Tokyo, Japan), and then glued to silicon frames and sealed in chambers maintained at low humidity using a desiccant (phosphorus oxide) until adhesion was complete (7 h).

To keep the outer-bark surface in contact with water, the space between the outer bark of 18 framed bark pieces and the silicone frame was filled with distilled water (Fig. 1). After 361 h, the distilled water was removed from the frames and any remaining water on the bark pieces was removed using a glass pipette. The bark weight was measured using an electronic balance (AUX-220; Shimadzu, Kyoto, Japan), and the moisture content [$u(t)$, %] of each piece was calculated as follows:

$$u(t) = \frac{w(t) - w_d}{w_d} \times 100, \tag{1}$$

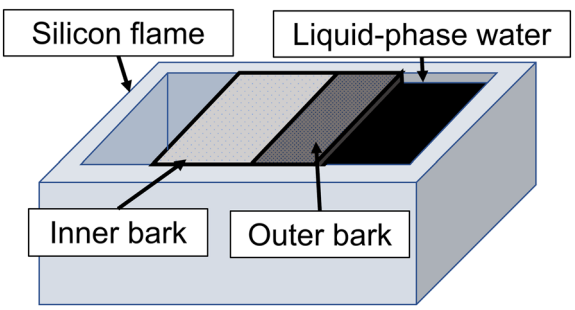

Fig. 1 Design of distilled-water and dye-solution water-permeation experiments. The outer-bark surfaces of bark pieces glued to silicone frames were permeated with either distilled water or dye solution. The chamber was maintained at a temperature of 20 °C and relative humidity ≥ 93%

where w_d is the dry weight after oven-drying (g) and $w(t)$ is the weight at time t (h) during the distilled-water permeation experiment.

In a separate experiment, six framed bark pieces were immersed in a 0.5% acidic fuchsin solution, maintaining contact between the dye solution and the outer bark, and placed in the chamber. After 336 h, a binocular stereomicroscope with a built-in camera (Stemi 305 cam, Carl Zeiss, Oberkochen, Germany) was used to photograph a cross section of each piece, at 100-s intervals. This experiment enabled the tracing of liquid-phase water permeation.

Both laboratory experiments were conducted at a constant temperature of 20 °C; the relative humidity was maintained at > 93% using the saturated salt solution (potassium nitrate) method. The distilled water or dye solution in the chamber was replenished at approximately 12-h intervals.

Evaluation of water absorption characteristics

The water (liquid-phase and vapor) absorption characteristics of the outer surfaces of the bark pieces were evaluated according to the change in weight of each sample throughout the experiment. In previous studies that have subjected woody materials, such as xylem and phloem, to water absorption, the amount of water absorbed in the early stages has increased proportionally with the square root of time; thus, the slope of the regression line has been used to evaluate permeation [33, 34]. Therefore, we performed linear regression of $u(t)$ against the square root of time ($t^{1/2}$) for each sample and calculated the slope (P_{rate}) and intercept (T) of the regression line using the least-squares method, as follows:

$$u(t) = P_{\mathrm{rate}} \times t^{\frac{1}{2}} + T\left(1 \leqq t^{\frac{1}{2}} \leqq A\right), \tag{2}$$

where P_{rate} is the rate of water absorption (% $t^{-1/2}$) and A is the endpoint of the linear regression range, i.e., the value closest to the mean value of the elapsed time ($t^{1/2}$) when the increasing trend significantly changed (bend point) in the sample plot (Fig. 2). We defined the maximum value of $u(t)$ as $u(t)$_max, and the difference between $u(t)$_max and T for each sample as the amount of water absorption (P_{amt}).

Evaluation of outer-bark shape in two and three dimensions

For each bark piece, the shape of the outer bark was quantitatively evaluated from a single cross-sectional photograph (magnification, 6×; resolution, 1280 pixels × 960 pixels) taken with a binocular stereomicroscope immediately before the distilled-water permeation experiment. OpenCV image-processing

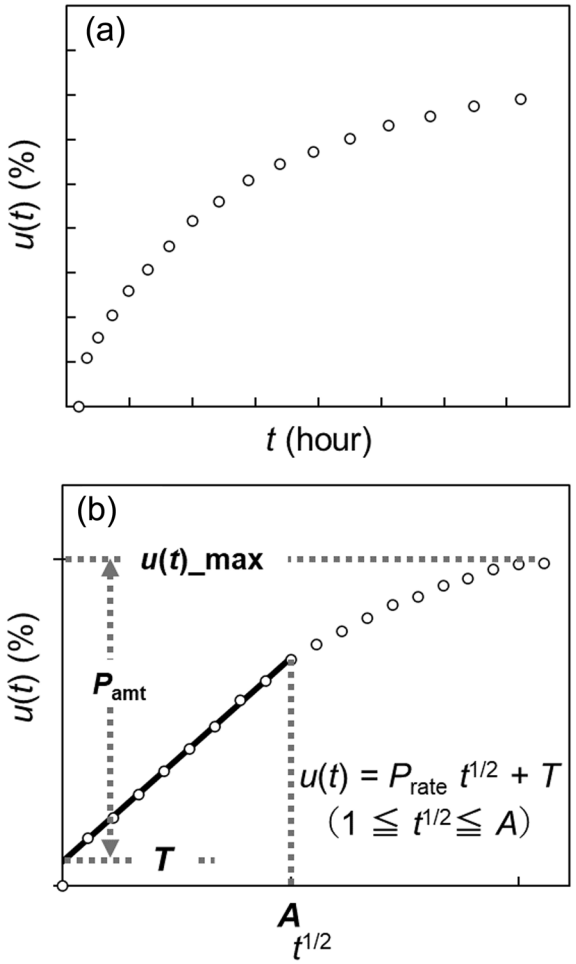

Fig. 2 The water absorption of bark pieces in the distilled-water permeation experiment. **a** Water content of a bark piece [$u(t)$, %] as a function of time (t). **b** Linear regression of the relationship between the square root of elapsed time ($t^{1/2}$) and $u(t)$ immediately after immersion ($1 \leq t^{1/2} \leq 9$)

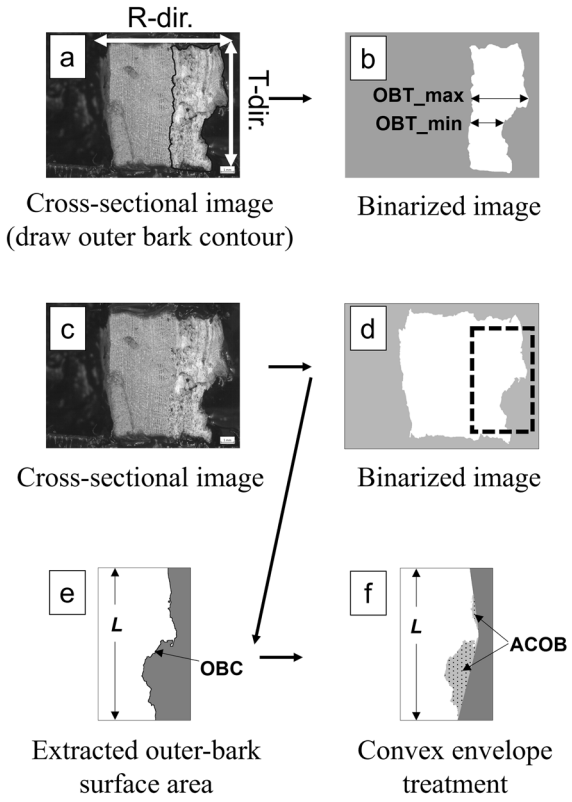

Fig. 3 Flowchart of image processing and calculation of the shape parameters of the outer bark. **a** Cross section of a bark piece. Black line indicates outer-bark edge. **b** Determination of outer-bark area (white shading). Measurement of outer-bark radial lengths and calculation of mean (OBT_avg), maximum (OBT_max), and minimum (OBT_min) thickness. **c** Cross section of a bark piece. **d** Determination of area of a bark piece (white shading). **e** Cutting of a piece (dashed line area in **d**), measurement of the outer-bark contour (OBC, black line), and calculation of the outer-bark surface roughness (ROBC). **f** Measurement of a convex envelope encompassing the total area of the outer-bark surface contour (ACOB), and calculation of the amount of outer-bark exfoliation (OBE). The scale length in a and c is 1.0 mm

software (version 4.5.4) was used to convert and extract information from the images. Threshold values were determined by referring to the histogram of red pixel numbers in the red–green–blue color space, and the edges and outer area of the bark pieces were determined by converting the photographs to binarized images (Fig. 3a–d). Because it was difficult to determine the boundary between the outer and inner bark using this method due to the lack of clear differences among red, green, and blue values, we determined the boundary visually to obtain the outer-bark area (Fig. 3a, b).

The thickness of the outer bark was calculated by aggregating radial lengths at 1-pixel intervals in the tangential direction in the outer-bark area to derive their mean (OBT_avg, mm), maximum (OBT_max, mm), and minimum (OBT_min, mm) values (Fig. 3b).

The outer-bark surface was extracted from the binarized image of each bark piece, and the length of the outer-bark surface contour (OBC, mm) was measured (Fig. 3e). The roughness of the outer-bark surface contour (ROBC, mm) was calculated as follows:

$$\mathrm{ROBC} = \mathrm{OBC} \times \frac{L}{10}, \tag{3}$$

where L is the tangential length of the area extracted from the binarized image (mm).

For each piece, a convex envelope was applied to the outer-bark surface contour, and the total area enclosed by the envelope and outer-bark surface contour (ACOB, mm^2) was measured (Fig. 3f). The amount of outer-bark

exfoliation (OBE, mm^2/mm^2) of each sample was calculated as follows:

$$\mathrm{OBE} = \frac{\mathrm{ACOB}}{(\mathrm{OBT\_avg} \times L)}, \quad (4)$$

where the product of OBT_avg and L is the approximate outer-bark area in the cross-section image of each sample.

To confirm that this method produced shape parameters of the outer bark that were representative of the overall shape of the outer bark, we also measured the bark surface in three dimensions as follows. Teak bark from the same individuals used in the distilled-water and dye-solution permeation experiments was cut to produce six pieces of bark with axial and tangential lengths of approximately 30 mm. For each sample, a portion of the outer-bark surface (approximately 10 mm in the axial and tangential directions) was measured using a three-dimensional (3D) microscope based on fringe projection (VR-3100, Keyence, Osaka, Japan) to obtain 3D shape data at a resolution of 0.024 mm/pixel (Additional file 1: Fig. S1a). From the 3D shape data, we set five straight tangential lines (width, 1 pixel) relative to the direction of the tree axis, at 0.25-mm intervals (Additional file 1: Fig. S1b). The contour of the outer-bark surface was drawn by connecting the radial coordinates at 1-pixel intervals along each tangential line (Additional file 1: Fig. S1c). ROBC and ACOB were derived from these contours, as described above.

Statistical analyses

To elucidate the relationship between outer-bark shapes and liquid-phase water permeation for each bark piece, we performed Pearson correlation analysis of the liquid-phase water absorption and shape parameters of the outer bark, followed by partial correlation analysis to evaluate the reliability of the correlations. All statistical analyses were performed using the *statsmodels* or *pengin* statistical package in the Python programming language.

Results

Water absorption characteristics

Because the mean value of the bend point in the $u(t)$ vs. $t^{1/2}$ curve was 9.33, A was set to 9.0. The coefficient of determination of the regression line exceeded 0.95. The slope of the regression line (P_{rate}) was significant ($p < 0.05$); however, the intercept (T) was significant only when one sample was excluded, so we considered this sample an outlier and excluded it from the analysis. The means ± standard errors (SEs) of $u(t)$_max, P_{rate}, T, and P_{amt} were 54.90 ± 7.70%, 3.50 ± 0.46%, 5.46 ± 0.76%, and 48.29 ± 7.67%, respectively (Fig. 4).

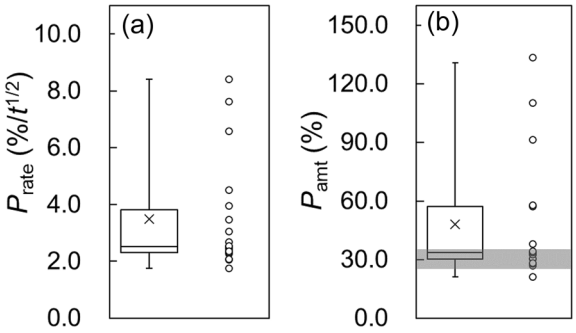

Fig. 4 Box-and-whisker plot of water-absorption characteristics. **a** Rate of water absorption (P_{rate}, % $t^{-1/2}$). **b** Water absorption (P_{amt}, %). Gray shading indicates the range of fiber-saturation points for wood (25–35%; [35])

Dye-solution permeation experiment

In the dye-solution permeation experiment, we observed large differences in the dyed areas in the cross sections of the bark pieces. Of two pieces with thin, smooth outer surfaces, the dye reached the innermost layer of the outer bark within 1 day in one piece (Fig. 5a) but barely permeated the surface within 14 days in the other (Fig. 5d). In pieces with thick, smooth outer surfaces, the dye reached the innermost layer of the outer bark in just over 2 days (Fig. 5b, e). In pieces with rough surfaces and signs of exfoliation, dye-solution permeation started from the exfoliated areas (Fig. 5c, f).

Shape parameters of the outer bark

Both ROBC and ACOB, calculated from five outer-bark surface contours obtained from the 3D shape data, were strongly positively correlated with the mean values of each contour ($R > 0.9$). The outer bark was characterized by fissures and thin exfoliation signs extending in the axial direction [31]. These results indicate that ROBC and OBE derived from cross-sectional photographs of teak bark pieces can be used to represent ROBC and OBE for the entire outer surface. OBT_avg, OBT_max, and OBT_min were also found to be representative of outer-bark thickness over the entire outer surface.

Our quantitative evaluation of the shape parameters of the outer bark using cross-sectional photographs of bark samples resulted in mean ± SE values for OBT_avg, OBT_max, and OBT_min of 2.96 ± 0.32, 3.87 ± 0.36, and 1.65 ± 0.25 mm, respectively. The means ± SEs of ROBC and OBE were 15.29 ± 0.99 mm and 10.68 ± 1.75, respectively.

Correlation analysis of liquid-phase water absorption and shape parameters of the outer bark

Correlation analysis of the shape parameters of the outer bark and P_{rate} or P_{amt} showed a significant correlation only

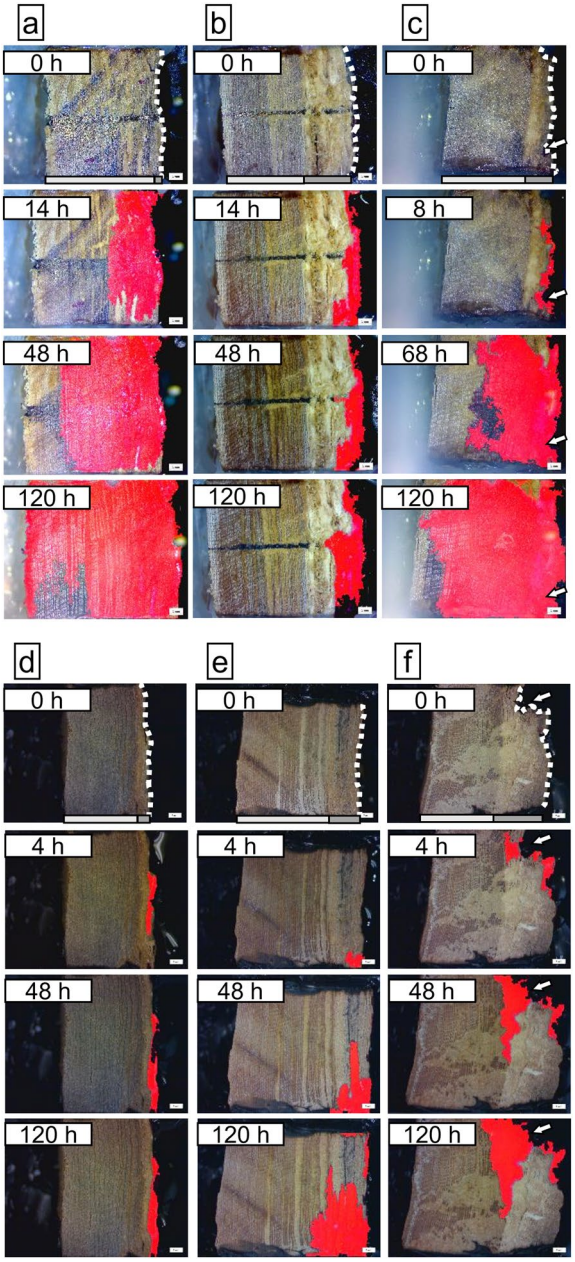

Fig. 5 Liquid-phase water permeation observations during dye-solution permeation experiments. Use bark pieces with **a**, **d** thin, smooth; **b**, **e** thick, smooth; and **c**, **f** rough outer-bark surfaces. White dashed lines indicate outer-bark surface contours; white and gray bars indicate inner and outer bark, respectively; white arrows indicate outer-bark exfoliation; red shading indicates dye permeation, as determined by image processing. The black lines marked on the centers of bark pieces a and b are reference lines for the measurement of the pieces' thickness. The scale length in all photos is 1.0 mm

between P_{rate} and OBT_min (Table 1). The partial correlation coefficient between P_{rate} and OBT_min had a low absolute value (Table 2), implying pseudo-correlation.

Table 1 Correlation coefficients between liquid-phase water absorption and shape parameters of the outer bark

	OBT_avg	OBT_max	OBT_min	ROBC	OBE
P_{rate}	−0.307	−0.152	−0.506*	0.373	0.726***
P_{amt}	−0.047	0.127	−0.382	0.470	0.560*
T	0.467	0.637**	0.017	0.866***	0.531*

* $p < 0.05$; ** $p < 0.01$; *** $p < 0.001$ (Student's t-test)

Thus, we found no clear correlation between liquid-phase water absorption on the outer-bark surface and outer-bark thickness in dried teak bark. P_{rate} and OBE were positively correlated (Table 1), and the absolute value of the partial correlation coefficient between P_{rate} and OBE was high (Table 2), indicating a clear relationship. T and ROBC were strongly positively correlated (Table 1), and their partial correlation coefficient was high (Table 2), further indicating a strong relationship.

Discussion

Interpretation of water-absorption characteristics

Previous studies that have evaluated the water-absorption parameters of woody materials have neglected the intercept of the linear regression of the square root of elapsed time vs. wood weight due to its low numerical value [33, 34]. However, T has not been neglected because its magnitude is equivalent to 10% of $u(t)$_max. The increasing trend of $u(t)$ at the beginning of our distilled-water permeation experiments may have been caused by water vapor absorption from the sides of the pieces other than the outer-bark surface. Some water may also have been retained on the outer surfaces when we pipetted the framed pieces for weight measurements. Therefore, T was determined to be an increase in the moisture content of the samples due to factors other than water absorption into the outer surface.

Main pathway of liquid-phase water permeation of teak stem surfaces

P_{rate} and P_{amt} differed among bark pieces that had different outer shapes (Fig. 4a, b). The equilibrium moisture content of pieces of teak bark at 20 °C and 93.0% relative humidity is 20.53% [30], and the moisture content at the fiber-saturation point of wood is generally 25–35% [35]. In the distilled water permeation experiment, most bark pieces had P_{amt} values below 35%, which could easily be attained through water vapor absorption. Among the remaining pieces, those with much higher P_{amt} values had likely undergone liquid-phase water permeation, because it is difficult to reach such high values through water vapor absorption alone (Fig. 4b). The results of the dye-solution permeation experiment show that the dye reached the inner bark

Table 2 Partial correlation coefficients between liquid-phase water absorption and shape parameters of the outer bark

	OBT_avg	OBT_max	OBT_min	ROBC	OBE	P_{rate}	P_{amt}	T
OBT_avg	1							
OBT_max	0.921***	1						
OBT_min	0.762**	−0.488	1					
ROBC	−0.246	0.345	−0.037	1				
OBE	−0.396	0.483	0.048	0.283	1			
P_{rate}	−0.107	−0.095	0.328	−0.286	0.612*	1		
P_{amt}	0.170	0.057	−0.455	0.113	−0.403	0.849***	1	
T	0.519	−0.450	−0.313	0.750**	0.031	0.294	−0.140	1

* $p < 0.05$; ** $p < 0.01$; *** $p < 0.001$ (Student's t-test)

of most pieces (Fig. 5). These findings indicate that in teak, liquid-phase water permeation occurs on the outer-bark surface, and water permeation of the stem surface may be spatially heterogeneous.

The results of our correlation and partial correlation analyses showed a significant positive correlation between P_{rate} and OBE (Tables 1, 2). P_{rate} was calculated according to the increase in liquid-phase water permeation within 81 h of the start of this experiment, and therefore reflects permeation within the short period after the outer-bark surface contacts the water. In the dye-solution experiment, the dye began to permeate the pieces at exfoliated surfaces, and rapidly reached the inner bark of pieces with rough outer bark (Fig. 5c, f). These results imply that the presence/absence and amount of exfoliation on the outer-bark surface significantly affect liquid-phase water permeation immediately after water contacts the surface. By contrast, P_{rate} and P_{amt} had no clear relationship with outer-bark thickness (OBT_avg, OBT_max, or OBT_min; Tables 1, 2). In bark pieces with smooth outer surfaces, the dye did not permeate even thin outer-bark layers (Fig. 5d), which implies that outer-bark thickness did not affect liquid-phase water permeation in this study.

The process of peeling the bark from the stem, cutting it into small pieces with a circular saw, and oven drying it may have led to the formation of microscopic cracks and pores that are not present in the outer bark of living trees. The occurrence of such cracks and pores may have caused physical damage to the periderm and provided a new pathway for the permeation of liquid-phase water from the outer-bark surface to the innermost periderm. This possibility is supported by the pattern of liquid-phase water permeation that we observed in bark pieces with less exfoliation (Fig. 5a, e). However, the rate of water absorption via the outer-bark surface correlated positively with the OBE, which does not reflect microscopic cracks and pores caused by bark processing. Thus, the presence of such microscopic cracks and pores should not affect the conclusion that outer bark exfoliation is the main pathway for liquid-phase water permeation.

These findings support our hypothesis that in dried teak bark, exfoliated outer-bark surfaces are the main pathway of liquid-phase water permeation, particularly within a short time of the bark surface contacting the water. Exfoliation of the outer bark, even when spontaneous, causes loss and breakage of the periderm [2]. As the phellem prevents the permeation of liquid-phase water and water vapor [11–14], the physical damage to the phellem caused by outer-bark exfoliation may contribute to liquid-phase water permeation via the outer-bark surface.

Factors increasing bark moisture content other than outer-surface permeation

ROBC and T were strongly correlated. Trees with rougher outer-bark surfaces have been found to have longer water-retention times [36], and *F. sylvatica* trees with smoother and thinner outer-bark surfaces have lower retention capacity [37]. Therefore, the water-retention capacity of the outer bark is affected by its surface roughness, implying that T may be related to the water-retention capacity of the stem surface in teak. However, we evaluated very small pieces of bark (1 cm^2), whereas those used in previous studies have been much larger, on the scale of ~ 15 and 25–50 cm^2 [36, 37]. Therefore, it is important to consider that our T estimates are not based on the effects of large exfoliations and fissures.

Conclusion

Our laboratory experiments using dried pieces of teak bark indicate that heterogeneous liquid-phase water permeation occurs via the outer-bark surface, with exfoliated surfaces acting as the main pathway for permeation. These findings imply that exfoliation may also be the main pathway for liquid-phase water permeation via stem surfaces in other tree species, and contribute

to our understanding of the association between frequent bark exfoliation and higher moisture absorption capacity. Furthermore, just as bark morphology can affect bark functions such as fire protection, drought, water storage, and tree body support [3–6], our findings imply that outer-bark shape affects other functions, such as water uptake, and may provide new insights into the determinants of bark morphology. However, the pattern of exfoliation and fissuring varies even among tree species whose outer bark consists of rhytidome [2, 38]. In addition, infrequently exfoliated outer bark formed only from periderm has lenticels that exchange water vapor and other gases [1, 2]. Lenticels are also involved in the absorption of liquid-phase water and water vapor via the stem surface [39]. Thus, the application of our method to a wider range of tree species will require the evaluation of outer bark characteristics using species-appropriate parameters. In addition, improved experimental methods, such as slower drying to prevent the formation of microscopic cracks and pores, are needed to ensure that sampled bark pieces have uniform water content. The drying process may significantly affect the water permeation pathways found in the innermost periderm of living trees, such as hydrophilic regions of the phellem cell wall and ray parenchyma [16, 22]. Isotopic labeling has been used to determine the absorption of rainwater and fog via the stem surfaces of living trees [19, 27]. In addition, transport pathways have been elucidated in living tree stems by freezing tree trunks that have absorbed labeled substances in liquid nitrogen and observing them through cryo-SEM/EDX analysis [40]. These techniques have enabled the tracing of the radial transport of water and minerals in the xylem tissue of living trees [41–43]. Thus, the combined use of stable isotope tracers and stem freezing to elucidate water permeation pathways in living bark and experiments using bark pieces to elucidate such pathways in dead outer-bark tissue would improve the understanding of water uptake on the stem surfaces of tree species with rhytidome structures.

Further research is needed to gain a more detailed understanding of water-uptake processes via tree-stem surfaces, including their contribution to tree water use and effects on the forest water cycle.

Abbreviations

A	End point of the range of linear regression
ACOB	Area of concave region within outer bark in cross section (mm^2)
L	Tangential width of outer-bark cutting area in cross section (mm)
OBC	Length of outer-bark contour in cross section (mm)
OBE	Amount of outer-bark exfoliation
OBT_avg	Mean thickness of outer bark (mm)
OBT_max	Maximum thickness of outer bark (mm)
OBT_min	Minimum thickness of outer bark (mm)
P_{amt}	Water absorption (%)
P_{rate}	Rate of water absorption (% $t^{-1/2}$)
ROBC	Roughness of outer-bark contours (mm)
t	Time (h)
T	Increase in water content due to causes other than water permeation (%)
$u(t)$	Water content of bark pieces (%)
$u(t)$_max	Maximum value of $u(t)$ (%)
w_d	Weight of bark pieces after oven drying (g)
$w(t)$	Weight of bark pieces at time t during the experiment (g)

Supplementary Information

The online version contains supplementary material available at https://doi.org/10.1186/s10086-023-02119-9.

Additional file 1: Figure S1. Three-dimensional (3D) shape data for outer-bark surfaces obtained through optical cutting. (a) 3D view of outer-bark surface. (b) Heat map based on radial length of outer-bark surface (dashed lines indicate target area for two-dimensional [2D] shape evaluation). (c) 2D data for outer-bark surface contours (black lines) in each target area based on tangential and radial coordinates of 3D shape data. The scale length in c images is 1.0 mm.

Acknowledgements

We thank the Forestry Faculty of Kasetsart University, the Thai Forest Industry Organization and the Aichi Center for Industry and Science Technology Industrial Research Center for their support. Dr. Takaharu Kameoka provided research advice.

Author contributions

HN performed the experiments and analyzed. HN and NM wrote the manuscript and interpreted the data. All authors contributed critically to the drafts and gave final approval for publication. All the authors read and approved the final manuscript.

Funding

This study was supported by Japan Society for the Promotion of Science KAKENHI grants (Numbers 24310018, 26304004 and 22K05746) and JST, the establishment of university fellowships towards the creation of science technology innovation (Numbers JPMJFS2122).

Availability of data and materials

The datasets used and/or analyzed during the current study are available from the corresponding author upon reasonable request.

Declarations

Competing interests

The authors declare that they have no competing interests.

Received: 1 September 2023 Accepted: 21 December 2023
Published online: 16 January 2024

References

1. Angyalossy V, Pace MR, Evert RF, Marcati CR, Oskolski AA, Terrazas T, Kotina E, Lens F, Mazzoni SC, Angeles G, MacHado SR, Crivellaro A, Rao KS, Junikka L, Nikolaeva N, Baas P (2016) IAWA list of microscopic bark features. IAWA J 37(4):517–615. https://doi.org/10.1163/22941932-20160151
2. Evert RF (2006) Esau's plant anatomy: meristems, cells, and tissues of the plant body - their structure, function, and development, 3rd edn. Wiley, Hoboken, pp 427–445
3. Romero C (2014) Bark: structure and functional ecology. Adv Econo Bot 17:5–25

4. Rosell JA (2019) Bark in woody plants: understanding the diversity of a multifunctional structure. Integr Comp Biol 59(3):535–547. https://doi.org/10.1093/icb/icz057
5. Rosell JA, Gleason S, Méndez-Alonzo R, Chang Y, Westoby M (2014) Bark functional ecology: evidence for tradeoffs, functional coordination, and environment producing bark diversity. New Phytol 201(2):486–497. https://doi.org/10.1111/nph.12541
6. Rosell JA, Olson ME (2014) The evolution of bark mechanics and storage across habitats in a clade of tropical trees. Am J Bot 101(5):764–777. https://doi.org/10.3732/ajb.1400109
7. Holmber A, Wadsö L, Stenström S (2016) Water vapor sorption and diffusivity in bark. Dry Technol 34(2):150–160. https://doi.org/10.1080/07373937.2015.1023310
8. Kajita H (1975) The bark-water relationship. Zairyo 24(264):862–866
9. Lequin S, Chassagne D, Karbowiak T, Gougeon R, Brachais L, Bellat JP (2010) Adsorption equilibria of water vapor on cork. J Agric Food Chem 58(6):3438–3445. https://doi.org/10.1021/jf9039364
10. White MS (1979) Water vapor diffusion through eastern hemlock periderm. Wood Fiber Sci 11(3):171–178
11. Groh B, Hübner C, Lendzian KJ (2002) Water and oxygen permeance of phellems isolated from trees: the role of waxes and lenticels. Planta 215(5):794–801. https://doi.org/10.1007/s00425-002-0811-8
12. Lendzian KJ (2006) Survival strategies of plants during secondary growth: barrier properties of phellems and lenticels towards water, oxygen, and carbon dioxide. J Exp Bot 57(11):2535–2546. https://doi.org/10.1093/jxb/erl014
13. Silva SP, Sabino MA, Fernandas EM, Correlo VM, Boesel LF, Reis RL (2005) Cork: properties, capabilities and applications. Int Mater Rev 50(6):345–365. https://doi.org/10.1179/174328005X41168
14. Vishwanath SJ, Delude C, Domergue F, Rowland O (2015) Suberin: biosynthesis, regulation, and polymer assembly of a protective extracellular barrier. Plant Cell Rep 34(4):573–586. https://doi.org/10.1007/s00299-014-1727-z
15. Katz C, Oren R, Schulze ED, Milburn JA (1989) Uptake of water and solutes through twigs of *Picea abies* (L.) Karst. Trees 3:33–37
16. Earles MJ, Sperling O, Silva LCR, McElrone AJ, Brodersen CR, North MP, Zwieniecki MA (2016) Bark water uptake promotes localized hydraulic recovery in coastal redwood crown. Plant Cell Environ 39(2):320–328. https://doi.org/10.1111/pce.12612
17. Liu J, Gu L, Yu Y, Huang P, Wu Z, Zhang Q, Qian Y, Wan X, Sun Z (2019) Corticular photosynthesis drives bark water uptake to refill embolized vessels in dehydrated branches of *Salix matsudana*. Plant Cell Environ 42(9):2584–2596. https://doi.org/10.1111/pce.13578
18. Carmichael MJ, White JC, Cory ST, Berry ZC, Smith WK (2020) Foliar water uptake of fog confers ecophysiological benefits to four common tree species of southeastern freshwater forested wetlands. Ecohydrol 13:e2240. https://doi.org/10.1002/eco.2240
19. Gimeno TE, Stangl ZR, Barbeta A, Saavedra N, Wingate L, Devert N, Marshall JD (2022) Water taken up through the bark is detected in the transpiration stream in intact upper-canopy branches. Plant Cell Environ 45(11):3219–3232. https://doi.org/10.1111/pce.14415
20. Berry ZC, Ávila-Lovera E, De Guzman ME, O'Keefe K, Emery NC (2021) Beneath the bark: assessing woody stem water and carbon fluxes and its prevalence across climates and the woody plant phylogeny. Front For Glob Chang 4:675299. https://doi.org/10.3389/ffgc.2021.675299
21. Van Stan JT, Dymond SF, Klamerus-Iwan A (2021) Bark-water interactions across ecosystem states and fluxes. Front For Glob Chang 4:660662. https://doi.org/10.3389/ffgc.2021.660662
22. Schönherr J, Ziegler H (1980) Water permeability of *Betula* periderm. Planta 147:345–354. https://doi.org/10.1007/BF00379844
23. Tonello KC, Campos SD, De Menezes AJ, Bramorski J, Mathias SL, Lima MT (2021) How is bark absorbability and wettability related to stemflow yield? Observations from isolated trees in the Brazilian Cerrado. Front For Glob Chang 4:650665. https://doi.org/10.3389/ffgc.2021.650665
24. Nunes E, Quilhó T, Pereira H (1999) Anatomy and chemical composition of *Pinus pinea* L. bark. Ann For Sci 56(6):479–484
25. Prislan P, Koch G, Schmitt U, Gričar J, Čufar K (2012) Cellular and topochemical characteristics of secondary changes in bark tissues of beech (*Fagus sylvatica*). Holzforschung 66(1):131–138. https://doi.org/10.1515/HF.2011.119
26. Loram-Lourenço L, Farnese FS, Alves RDFB, Dario BMM, Martins AC, Aun MA, Batista PF, Silva FG, Cochard H, Franco AC, Menezes-Silva PE (2022) Variations in bark structural properties affect both water loss and carbon economics in neotropical savanna trees in the Cerrado region of Brazil. J Ecol 110(8):1826–1843. https://doi.org/10.1111/1365-2745.13908
27. Mayr S, Schmid P, Laur J, Rosner S, Charra-Vaskou K, Dämon B, Hacke UG (2014) Uptake of water via branches helps timberline conifers refill embolized xylem in late winter. Plant Physiol 164(4):1731–1740. https://doi.org/10.1104/pp.114.236646
28. Laur J, Hacke UG (2014) Exploring *Picea glauca* aquaporins in the context of needle water uptake and xylem refilling. New Phytol 203(2):388–400. https://doi.org/10.1111/nph.12806
29. Teskey RO, McGuire MA (2005) CO_2 transported in xylem sap affects CO_2 efflux from *Liquidambar styraciflua* and *Platanus occidentalis* stems, and contributes to observed wound respiration phenomena. Trees 19(4):357–362. https://doi.org/10.1007/s00468-004-0386-z
30. Matsunaga H, Matsuo N, Nakai T, Yoshifuji N, Tanaka N, Tanaka K, Tantasirin C (2021) Absorption and emission of water vapor from the bark of teak (*Tectona grandis*), a deciduous tree, in a tropical region during the dry season. Hydrol Res Let 15(3):58–63. https://doi.org/10.3178/hrl.15.58
31. Baptista I, Miranda I, Quilhó T, Gominho J, Pereira H (2013) Characterisation and fractioning of *Tectona grandis* bark in view of its valorisation as a biorefinery raw-material. Ind Crops Prod 50:166–175. https://doi.org/10.1016/j.indcrop.2013.07.004
32. Schönherr J, Schmidt HW (1979) Water permeability of plant cuticles. Planta 144:391–400. https://doi.org/10.1007/bf00391583
33. Haishi T (1980) Basic modes of water absorption by woods I. The behaviors of bound and free water during penetration into wood. Mokuzai Gakkaishi 26(8):510–518
34. Yata S, Mukudai J, Kajita H (1980) Penetration of liquid into the air-dried hardwood. Sci Rep Kyoto Pref Univ Agr 33:73–85 (**in Japanese with English Summary**)
35. Terasawa M (2004) Philosophy of lumber drying, 2nd edn. Kaiseisha, Kaiseisha, p 594
36. Levia DF, Herwitz SR (2005) Interspecific variation of bark water storage capacity of three deciduous tree species in relation to stemflow yield and solute flux to forest soils. CATENA 64(1):117–137. https://doi.org/10.1016/j.catena.2005.08.001
37. Fritz Ö, Brunet J, Caldiz M (2009) Interacting effects of tree characteristics on the occurrence of rare epiphytes in a Swedish beech forest area. Bryologist 112(3):488–505. https://doi.org/10.1639/0007-2745-112.3.488
38. Whitmore TC (1962) Studies in systematic bark morphology: I. Bark morphology in Dipterocarpaceae. New Phytol 61(2):191–207. https://doi.org/10.1111/j.1469-8137.1962.tb06288.x
39. Rosner S, Morris H (2022) Breathing life into trees: the physiological and biomechanical functions of lenticels. IAWA J 43(3):234–262. https://doi.org/10.1163/22941932-bja10090
40. Utsumi Y, Sano Y (2014) Freeze stabilization and cryopreparation technique for visualizing the water distribution in woody tissues by X-Ray imaging and cryo-scanning electron microscopy. In: Kuo J (ed) Electron microscopy: method and protocols Methods in molecular biology, vol 1117. Springer, New York, pp 677–688. https://doi.org/10.1007/978-1-62703-776-1_30
41. Kuroda K, Yamane K, Itoh Y (2018) Cellular level in planta analysis of radial movement of artificially injected cesium in *Cryptomeria japonica* xylem. Trees 32(6):1505–1517. https://doi.org/10.1007/s00468-018-1729-5
42. Kuroda K, Yamane K, Itoh Y (2020) Radial movement of minerals in the trunks of standing Japanese Cedar (*Cryptomeria Japonica* D. Don) trees in summer by tracer analysis. Forests 11(5):562. https://doi.org/10.3390/f11050562
43. Kuroda K, Yamane K, Itoh Y (2021) In planta analysis of the radial movement of minerals from inside to outside in the trunks of standing Japanese cedar (*Cryptomeria japonica* D. Don) trees at the cellular level. Forests 12(2):1–14. https://doi.org/10.3390/f12020251

Publisher's Note